



**QUEEN'S  
UNIVERSITY  
BELFAST**

## **An assessment of wind and wave climate as potential sources of renewable energy in the nearshore Shenzhen coastal zone of the South China Sea**

Chen, X., Wang, K., Zhang, Z., Zeng, Y., Zhang, Y., & O'Driscoll, K. (2017). An assessment of wind and wave climate as potential sources of renewable energy in the nearshore Shenzhen coastal zone of the South China Sea. *Energy*, 134, 789-801. <https://doi.org/10.1016/j.energy.2017.06.043>

**Published in:**  
Energy

**Document Version:**  
Peer reviewed version

**Queen's University Belfast - Research Portal:**  
[Link to publication record in Queen's University Belfast Research Portal](#)

### **Publisher rights**

Copyright 2017 Elsevier.

This manuscript is distributed under a Creative Commons Attribution-NonCommercial-NoDerivs License (<https://creativecommons.org/licenses/by-nc-nd/4.0/>), which permits distribution and reproduction for non-commercial purposes, provided the author and source are cited.

### **General rights**

Copyright for the publications made accessible via the Queen's University Belfast Research Portal is retained by the author(s) and / or other copyright owners and it is a condition of accessing these publications that users recognise and abide by the legal requirements associated with these rights.

### **Take down policy**

The Research Portal is Queen's institutional repository that provides access to Queen's research output. Every effort has been made to ensure that content in the Research Portal does not infringe any person's rights, or applicable UK laws. If you discover content in the Research Portal that you believe breaches copyright or violates any law, please contact [openaccess@qub.ac.uk](mailto:openaccess@qub.ac.uk).

### **Open Access**

This research has been made openly available by Queen's academics and its Open Research team. We would love to hear how access to this research benefits you. – Share your feedback with us: <http://go.qub.ac.uk/oa-feedback>

# An assessment of wind and wave climate as potential sources of renewable energy in the nearshore Shenzhen coastal zone of the South China Sea

Xinping Chen<sup>a</sup>, Kaimin Wang<sup>b</sup>, Zenghai Zhang<sup>c</sup>, Yindong Zeng<sup>d</sup>, Yao Zhang<sup>a,\*</sup>, Kieran O'Driscoll<sup>e</sup>

<sup>a</sup>*National Marine Hazard Mitigation Service of State Oceanic Administration, Beijing 100194, China.*

<sup>b</sup>*Shenzhen Marine Monitoring Forecasting Center, Shenzhen 518067, China.*

<sup>c</sup>*National Meteorological Center of China Meteorological Administration, Beijing 100081, China.*

<sup>d</sup>*Marine Forecasting Center of Fujian Province, Fuzhou 350003, China.*

<sup>e</sup>*School of Natural and Built Environment, Queen's University Belfast, Belfast, Northern Ireland, UK.*

---

## Abstract

In this study, nearshore wind and wave climates and their potential as renewable energy sources are evaluated by means of buoy observational data for the Shenzhen coastal region. Six buoys were originally deployed in the region by the city local government of China in 2014, and are located in different areas of the study region, including Dapeng Bay, Daya Bay, Shenzhen Bay. The waters in these areas are relatively shallow, ranging in depth between about 3-22 m. The results show that during 2014-2016, annual mean wind speeds (at 2.5 m above the sea surface) in the region varied between 3.1-4.1  $\text{ms}^{-1}$ , leading to wind powers between 37-94  $\text{W m}^{-2}$ ; significant wave

---

\*Corresponding author.

*Email addresses:* xinp.chen@foxmail.com (Xinping Chen),  
yaozhang\_zhang@126.com (Yao Zhang)

heights were mostly less than 1 m, while wave energy periods were mostly in the range 3–7 s. As a result, wave power was mostly less than  $1.0 \text{ kW m}^{-1}$ . It is concluded that the potential of wave energy as a renewable resource at the buoy locations was very small. This may be due to the fact that, first, water depth is very shallow, and, secondly, the buoys are located in bays where the sea is somewhat semi-enclosed, all of which are not favourable for the development of wind waves.

*Keywords:* Wave climate, Wave energy, Shenzhen, Wind climate, Wind energy, the South China Sea

---

## 1. Introduction

Energy has become one of the hottest words in China. On the one hand, the demand for energy in China is rapidly increasing, since China has become the largest energy consumer and producer in the world (US Energy Information Administration, EIA; <http://www.eia.gov/>), whereas on the other, energy is closely associated with the environment. For example, coal and oil consumption in the country has resulted in very seriously bad air pollution impacts and environmental problems, which have been reported on in countless situations. Air pollution and smog in China have become one of the most contentious issue for the international media. Hundreds of millions of people in the world's most populous country are suffering the effects of this pollution, which is putting a lot of pressure on environmental and public health conditions in China. To mitigate these problems, China has to accelerate the adjustment of energy structure and to increase the share of clean sources in its energy mix. According to China's Action Plan for the Prevention and

16 Control of Air Pollution [1], China desires to reduce coal consumption to less  
17 than 65% in terms of total energy consumption by 2017.

18 China has a very long coastline, possessing rich ocean resources, which  
19 attach great importance to marine development and exploitation of renewable  
20 energy. As important renewable types, ocean wind and wave energy not only  
21 provide China with energy sources, but also resources with which to address  
22 and relieve the challenge of energy demands with respect to the environment  
23 , while implementing a sustained development strategy. As [2] mentioned,  
24 renewables can also provide tools to address many pressing needs, including  
25 improving energy security, reducing human health problems, and mitigating  
26 against greenhouse gas emissions.

27 In recent times (decades), previous researchers have made great contribu-  
28 tions toward the assessment of wind/wave energy potential for various seas  
29 in many regions and countries, based on the analysis of wind/wave data col-  
30 lected from buoys, remote sensing, numerical hindcasts, and combinations of  
31 these sources. Included among these are the following studies: for the UK  
32 [3, 4], Portugal [5–7], Sweden [8], Belgium [9], Spain [10–13], Ireland [14, 15],  
33 Europe [16], the North Sea [9], the Baltic Sea [17, 18], the Red Sea [19], the  
34 Caribbean [20], Australia [21, 22], Canada [23], Iran [24], India [25–29], Korea  
35 [30], Singapore [31], Chile [32], the Hawaiian islands [33, 34], Southern New  
36 England [35], California [36, 37], the Atlantic coast of the southeastern USA  
37 [36, 38], the US Pacific Northwest [39], as well as for the global ocean (e.g.,  
38 [40–44]). In addition, wave/wind energy resource assessment has also been  
39 conducted for China [e.g., 45–54], and also including for Hongkong [55–58].

40 The region of interest in the present study is near the coast of Shenzhen,

41 located at the northern extreme of the South China Sea. Shenzhen shares a  
42 border with Hong Kong to the south, is 160 km south of the provincial capital  
43 of Guangzhou, and 70 km south of the industrial city of Dongguan. To the  
44 west, the resort city of Zhuhai is a 60 km away, (see Fig. 1). Shenzhen was  
45 the earliest of the five special economic zones in China, originally established  
46 in 1979, and was given the right of provincial-level economic administration.  
47 Since then, it has been one of the fastest growing cities in the world, and  
48 eventually became one of the largest cities in the Pearl River Delta region  
49 from the one-time small fishing village, and one of the economic powerhouses  
50 of China, as well as of the largest manufacturing bases in the world. As a  
51 result of this tremendous economic growth, the demand for energy is no  
52 doubt correspondingly rapidly increasing. The first nuclear power plant in  
53 China was built in the coast of Daya Bay (see Fig. 1), a coastal region of  
54 Shenzhen. However, relative to the economic growth, the marine develop-  
55 ment of Shenzhen has fallen far behind. It wasn't until 2014 that the city  
56 local government put buoys in the surrounding waters to observe and moni-  
57 tor the atmospheric and hydrodynamic climate of the region, and for use in  
58 marine and meteorology environmental studies and forecasting, and so on.  
59 The locations of the buoys have been shown to be reasonably representative  
60 of the hydrodynamic climate of different areas in this region, in a limited ex-  
61 penditure, and, from these, 6 buoy locations were selected (see section 2 for  
62 details). This was a great progression and good start for marine observations  
63 and monitoring for this region.

64 By means of data collected from six buoys located in the nearshore Shen-  
65 zhen zone, this study aims to evaluate wind and wave climate for the region,

66 in terms of wind speed and direction, wave height, wave period and wave di-  
67 rection. The potential of wind and wave energy as resources is assessed based  
68 on buoy observations for the period 2014–2016. Location of the area of in-  
69 terest and accumulated data at each of the six buoys, and also bathymetry  
70 of the region are described in detail in section 2, where the methods for es-  
71 timating wind and wave power are also presented. Wind and wave resource  
72 variability in the region are investigated and discussed in section 3. Finally,  
73 conclusions are presented in section 4.

## 74 2. Data and methods

### 75 2.1. Study area and buoy data

76 The region of wind and wave energy resource under investigation extends  
77 from 22.0°N–23.0°N and 113.5°E–114.5°E (Fig. 1), and includes the entire  
78 nearshore region of Shenzhen adjacent to Hong Kong. Six buoys, acquired  
79 from Shenzhen Marine Monitoring Forecasting Center, are available in the  
80 study region, and their locations and corresponding mean water depths are  
81 listed in Table 1. Data from these buoys represent the wind and wave cli-  
82 mate for different areas of the Shenzhen coastal region, mainly to monitor  
83 atmospheric and hydrodynamic changes in this region and also to be used for  
84 marine environmental investigating, forecasting, etc. The study area consists  
85 of the waters extending from Shenzhen Bay in the northwest, southward and  
86 eastward containing waters surrounding Hong Kong to Dapeng Bay, east of  
87 Hong Kong and further east to include Daya Bay. The six buoys are located  
88 very close to shore in very shallow water across the three bays: B1 is located  
89 in the northwest end of Dapeng Bay in water depth of about 11 m; B2 is also

90 located in Dapeng Bay, close to the western side of Dapeng Peninsula; B3  
91 is located in Aozaixia Bay in inner Daya Bay in water depth of only about  
92 3 m; B5 is situated in southern Daya Bay (water depth: 12 m); B4 is located  
93 in the relatively open area off the tip of Dapeng peninsula in water depth of  
94 about 22 m; and B6 is located in inner Shenzhen Bay, in a relatively narrow  
95 and closed area with water depth only 3 m.

96 The six buoys have been in operation since April 2014. Wave data were  
97 provided hourly, consisting of wave parameters, including wave height, period  
98 and direction. However, some wave data were not recorded over a span  
99 of several days, and data gaps for each buoy can be inferred from Fig. 7.  
100 Significant wave height ( $H_s$ ), which is identical to the average of the highest  
101 one-third of all wave heights recorded during each wave acquisition, is utilized  
102 and analyzed for wave energy assessment in this study, while the measured  
103 wave period acquired from buoy measurements refers to mean wave period,  
104  $T_m$ . However, only buoys B1–B4 and B6 provided records of wind data  
105 (at 2.5 m above sea surface), including wind speed and direction at quarter-  
106 hourly intervals, except for B4 (mainly half-hourly). Wind direction at B6  
107 was also missed.

## 108 *2.2. Analytical methods and approach*

109 Wind power is defined as the power per unit section perpendicular to  
110 wind flow, and is computed in this study by the following equation [52]:

$$W = \frac{1}{2}\rho_a V^3, \quad (1)$$

111 in which  $W$  is wind power in units of  $\text{W m}^{-2}$ ,  $V$  is wind speed (unit:  $\text{m s}^{-1}$ ),  
112 and  $\rho_a$  is air density taken as  $1.292 \text{ kg m}^{-3}$  and corresponding to that close

113 to the sea surface in the region of interest in this study.

114 It was noticed that, for wave power calculations and assessments, the  
115 widely used wave period is the so-called wave energy period,  $T_e$ , instead of  
116  $T_m$ .  $T_e$  can be defined as  $T_e \equiv T_{-10} = \frac{m_{-1}}{m_0}$ , in which  $m_n$  is the  $n^{\text{th}}$  moment  
117 of spectral density, i.e.,  $m_n = \int_0^{2\pi} \int_0^\infty f^n S(f, \theta) df d\theta$ , and here  $f$  is the wave  
118 frequency,  $\theta$  is the wave direction, and  $S(f, \theta)$  is the 2D wave spectrum. In  
119 general, the observed wave period measured by buoys for real sea states is  
120 rarely specified by  $T_e$ , but is specified in terms of the mean wave period  $T_m$ , or  
121 in terms of the peak period  $T_p$ .  $T_e$  is often estimated by means of its relation  
122 to other observational wave periods, such as  $T_m$  and  $T_p$ , when the spectral  
123 density is unknown [40]. Therefore, the relationship between  $T_e$  and  $T_p$  can  
124 be estimated by the formula  $T_e = \alpha T_p$ , in which  $\alpha$  depends on the shape of  
125 the wave spectrum used to define the sea state. The relationship between  
126  $T_p$  and  $T_e$  used in this study is computed by a conservative approximation  
127 that  $T_e = 0.9T_p$ , according to the study of [40]. This relationship has been  
128 widely adopted in assessing the wave energy resource such as off the coast of  
129 Canada [23], in the North Sea [9], and for the global ocean [40] as well as for  
130 the offshore wave power in the East China Sea [54].

131 Based on the study of [8, 10–12, 28, 41, 54], the wave power,  $P$ , known  
132 as wave energy flux as well, is calculated by the following expression

$$P = \frac{\rho_w g^2}{64\pi} H_s^2 T_e, \quad (2)$$

133 where  $\rho_w$  represents sea water density taken as  $1025 \text{ kg m}^{-3}$ , the average  
134 sea water density in the study area. Since  $T_p$  was not provided in the buoy  
135 records acquired in this study,  $T_m$  was used to estimate the wave power in the  
136 region of interest. Following the study of [54, 59], the relationship between



137  $T_m$  and  $T_p$  is adopted as  $T_p = 1.2T_m$ , and as a result,  $T_e$  investigated in the  
138 present study is computed by means of  $T_m$  as  $T_p = 0.9 \times 1.2T_m = 1.08T_m$ .

### 139 **3. Results and Discussion**

#### 140 *3.1. Wind climate and assessment of wind energy potential*

141 To assess the wind climate in the Shenzhen coastal region, the time series  
142 of wind speeds based on the buoy measurement data (B1–B4 and B6) for the  
143 period 2014–2016 is plotted by Fig. 2. It can be observed that wind speeds  
144 in the study area were mostly less than  $8 \text{ m s}^{-1}$  for the 5 buoys except B4  
145 buoy, where the wind speed was generally less than  $10 \text{ m s}^{-1}$ ; relatively high  
146 wind speeds of greater than  $15 \text{ m s}^{-1}$  occurred occasionally. Based on Eq. 2,  
147 Fig. 3 displays the calculated wind power for the 5 buoys. It shows that the  
148 wind power for the 5 buoys (except B4) was mostly less than  $300 \text{ W m}^{-2}$ ,  
149 while B4 shows relatively larger wind speeds, with values mostly smaller  
150 than  $500 \text{ W m}^{-2}$ . Large wind power values of more than  $3500 \text{ W m}^{-2}$  can  
151 occasionally be found in the observed time.

152 The fundamental characteristics of wind energy resources, in terms of  
153 the annual mean wind speed with its standard deviation ( $(V_{mean} \pm \text{std.dev.})$ ),  
154 maximum wind speed ( $V_{max}$ ), annual mean and maximum wind power (i.e.,  
155  $W_{mean}$  and  $W_{max}$ ), is summarized in Table 1. In Dapeng bay, represented  
156 by buoys B1 and B2, the annual mean wind speed during 2014–2016 was  
157  $3.1 \text{ m s}^{-1}$ , and in Daya Bay, represented by B3,  $V_{mean}$  was  $3.4 \text{ m s}^{-1}$ ; simi-  
158 larly, in Shenzhen bay, as B6 shows,  $V_{mean}$  was  $3.6 \text{ m s}^{-1}$ ; relatively stronger  
159 wind speed was found at B4, with mean wind speed of  $4.1 \text{ m s}^{-1}$ . In ac-  
160 cordance with the mean wind speed, the annual mean wind power,  $W_{mean}$ ,

161 at B1 and B2 was, respectively,  $58 \text{ W m}^{-2}$  and  $37 \text{ W m}^{-2}$ , and  $W_{mean}$  was  
162 around  $50 \text{ W m}^{-2}$  in Daya bay and Shenzhen bay, highest  $W_{mean}$  among the  
163 buoys was found at B4 with value of  $94 \text{ W m}^{-2}$ .  $V_{mean}$  averaged at the buoys  
164 was about  $3.5 \text{ m s}^{-1}$ , leading to an average  $W_{mean}$  of around  $58 \text{ W m}^{-2}$  for  
165 2014–2016.

166 For the period 2014–2016, maximum wind speed,  $V_{max}$ , at B1, B2, and  
167 B4 was, respectively,  $17.5 \text{ m s}^{-1}$ ,  $17.6 \text{ m s}^{-1}$ ,  $17.1 \text{ m s}^{-1}$ , leading to wind power  
168 of more than  $3000 \text{ W m}^{-2}$ , while  $V_{max}$  was relatively smaller at B3 and B6,  
169 with values of  $15.66 \text{ m s}^{-1}$  and  $15.7 \text{ m s}^{-1}$ , respectively, giving a corresponding  
170  $W_{max}$  of over  $2300 \text{ W m}^{-2}$ .

171 It is noted that the study region is influenced by tropical cyclones (TCs;  
172 normally called typhoons in China) relatively frequently, and they have been  
173 reported many times. Therefore, the variance of maximum wind speeds can  
174 be quite large for different time periods. Maximum wind speed depends  
175 greatly on the extent and degree of the TC effects. For example, for the  
176 period 2014–2016, 3 TCs passed through the study region that had much  
177 influence it, see Fig. 4. The periods of these TCs are plotted in Fig. 2, and  
178 it is observed that wind speeds in these time were relatively high. TCS are  
179 normally classified into different categories. In China, in accordance with  
180 the World Meteorological Organization’s recommendation, the classification  
181 is divided into 6 categories by the classification of TCs standardization of  
182 China (GB/T19201–2006 [60]), in terms of wind speed averaged over a pe-  
183 riod of 10 minutes near the center of the TC. The six classifications are  
184 as follows: Tropical Depression (TD;  $10.8–17.1 \text{ m s}^{-1}$ ); Tropical Storm (TS;  
185  $17.2–24.4 \text{ m s}^{-1}$ ); Severe Tropical Storm (STS;  $24.5–32.6 \text{ m s}^{-1}$ ); Typhoon

186 (TY;  $32.7\text{--}41.4\text{ m s}^{-1}$ ); Severe Typhoon (STY;  $41.5\text{--}50.9\text{ m s}^{-1}$ ); and Super  
187 Typhoon (SuperTY;  $\geq 51.0\text{ m s}^{-1}$ ). Fig. 4 shows that TCs Nida (No. 1604)  
188 and Haima (No. 1622) were in the classification of STY when they landed  
189 (around Aug. 2 and Oct. 21 in 2016, respectively), and correspondingly, the  
190 wind speeds could reach up to  $15\text{ m s}^{-1}$  at B1, B2 and B4 locations, while  
191 they were relatively small (about  $10\text{ m s}^{-1}$ ) at locations B3 and B6. Linfa  
192 (No. 1510) was much weaker when it came to the Shenzhen region, and  
193 its influence on wind speed was much less. The other 3 TCs displayed in  
194 Fig. 4 were relatively far from the study region, but their influence is still  
195 seen: wind speed at the 4 buoys were all relatively large with values reaching  
196  $15\text{ m s}^{-1}$ , in the influence of the Kalmaegi (No. 1415); the other two TCs  
197 were also evident for the wind speeds in the study area.

198 The seasonal and monthly mean wind speed variations at the wind buoys  
199 in the study area are presented by Fig. 5. For the present study, the four  
200 boreal seasons are winter (December–February), spring (March–May), sum-  
201 mer (June–August), and Autumn (September–November). The monthly  
202 wind speeds over the period 2014–2016 varied from about  $2\text{--}6\text{ m s}^{-1}$ , with  
203 different variability found at each of the buoys. Highest monthly mean wind  
204 speeds occurred at station B4, with values of about  $5.6\text{ m s}^{-1}$  in November  
205 2015, followed by station B1 ( $5.2\text{ m s}^{-1}$  in December 2014). However, at lo-  
206 cation B6 in Shenzhen Bay, the largest monthly wind speed was not found  
207 in winter, but in June 2015 ( $4.3\text{ m s}^{-1}$ ), followed by June 2016 ( $4.2\text{ m s}^{-1}$ ),  
208 while the smallest monthly value was reported in October 2016.

209 Corresponding to wind speeds, monthly mean wind powers at the 5 buoy  
210 locations varied from  $20\text{ W m}^{-2}$  to  $200\text{ W m}^{-2}$ : relatively large wind powers

211 can be found in autumn and winter months at B1 and B4; while at B6 wind  
212 powers in June and July were larger than those in winter months.

213 Fig. 5 also shows that the variation of monthly mean wind speeds and  
214 powers within a year was largest at B1, followed by B4, and was smallest  
215 at B3. Furthermore, no coincident seasonal variability was found in the  
216 winds and the wind powers at any of the buoy locations for 2014–2016. Of  
217 these, stations B1 and B4 show similar seasonality: winds and wind powers  
218 were relatively large in autumn and winter, and were smaller in the spring  
219 and summer months; however, B2 and B3 locations did not show evident  
220 seasonality. Note that the data in some months for B2 was lacking, which  
221 may influence the accuracy of its seasonality. On the contrary, B6 location  
222 shows opposite seasonality when compared with B1 and B4 during the study  
223 period: winds and wind powers were relatively large in spring and summer,  
224 and were smaller in autumn and winter months.

225 Besides wind speed, wind direction is another important parameter in  
226 wind energy assessment. For the data collected at the 6 buoys, only that at  
227 buoys B1–B4 include wind direction data. Wind direction and wind speed  
228 for different seasons at the 4 buoys is presented in terms of a wind rose figure,  
229 Fig. 6. It can be seen that variability in wind direction is different for the  
230 4 buoy locations. At location B1, in winter, easterly winds prevailed (about  
231 31%), followed by winds directed from the ESE (about 28%), and occasionally  
232 from the ENE and N (about 7%), whereas westerly winds are least frequent  
233 (less than 5%); in spring, prevailing direction was from the II quadrant,  
234 i.e., from E to S, with least occurrence also from the west; in autumn and  
235 winter, winds were mostly southerly, followed by SSE and SSW directions,

236 respectively, and winds from land, i.e., from the IV and I quadrants, provided  
237 the smallest contribution to the wind energy at B1. For B2, the prevailing  
238 wind direction was easterly in all seasons (over 45%), followed by ENE, and  
239 lowest occurrence occurred from SE to NW. At location B3 in Daya Bay, for  
240 all seasons the largest contribution to wind energy resources was provided  
241 by southerly winds, and SSE and SSW winds also provided considerable  
242 contributions. At the B4 location, the prevailing wind direction varied for  
243 all seasons, with almost all occurrence from each direction being less than  
244 15%: in winter, most winds were from the the I quadrant followed by the  
245 II quadrant; W (about 16%) prevailed in spring, followed by WSW (14%)  
246 and WNW (13%); southerly winds prevailed in autumn, and winds from E  
247 to W accounted for more than 75% of occurrence; in autumn, most winds  
248 were from the III quadrant.

249 The occurrence of wind speed at the 4 buoy locations during 2014–2016  
250 can also be observed from Fig. 6. For B1, the occurrence of wind with speed  
251 less than  $5 \text{ m s}^{-1}$  was, respectively, about 85%, 88%, 90%, and 70% in the 4  
252 seasons (winter, spring, summer and autumn); relatively large wind speeds  
253 of over  $8 \text{ m s}^{-1}$  are mostly found in autumn (about 10%), followed by winter  
254 (about 3%). For B2, around 86% of wind speed was less than  $5 \text{ m s}^{-1}$  in all  
255 seasons except spring, when it was around 80%; the occurrence of wind speed  
256 greater than  $8 \text{ m s}^{-1}$  was always less than 1% of the time in all seasons. At B3  
257 wind speed was less than  $5 \text{ m s}^{-1}$  80% of the time, while wind speed greater  
258 than  $8 \text{ m s}^{-1}$  also occurred relatively rarely (less than 2% for all seasons).  
259 Among the 4 buoys wind speed was greatest at B4, where wind speeds were  
260 over  $5 \text{ m s}^{-1}$  in winter and autumn about 45% of the time, and 20% of the

261 time in summer and spring; the occurrence of wind speed over  $8 \text{ ms}^{-1}$  was,  
262 respectively, about 10%, 3.6%, 3.8%, and 1.5% in winter, spring, summer  
263 and autumn.

### 264 3.2. Wave climate and assessment of wave energy potential

265 In this section, wave state in terms of observed wave height and calculated  
266 wave energy period is analyzed. Time series of significant wave height,  $H_s$ ,  
267 and wave energy period,  $T_e$ , at the six buoys considered in this study are  
268 presented in Fig. 7. It can be seen from this figure that  $H_s$  is relatively low  
269 for most of the period 2014–2016. At the 6 buoy stations,  $H_s$  was less than  
270 1 m, most of the time, and was even less than 0.5 m at buoy stations B2, B3,  
271 and B6. It is not surprising that  $H_s$  is small in this region, since, first of all,  
272 water depth is very small, and, secondly, the buoys are located in bays that  
273 are somewhat semi-closed, all of which are not favorable for the development  
274 of wind waves. Among these six buoys,  $H_s$  at B4 was relatively higher than  
275 that at the others, which is to be expected since the water is deepest here  
276 while being closer to the open South China Sea. Relatively higher values  
277 exceeding 2 m are found only in some rare cases due to relatively strong winds  
278 caused by tropical cyclones passing through the region, see discussion above.  
279 For the period 2014–2016, no extreme waves (e.g.,  $H_s > 10 \text{ m}$ ) were observed,  
280 even during periods of influence from tropical cyclones passing through.

281  $T_e$  at the buoys is also presented in Fig. 7. In inner Dapeng Bay, repre-  
282 sented by B1 and B2,  $T_e$  mostly varies between 3 s and 7 s, with occasional  
283 values of more than 10 s. Similarly, at B5, in Daya bay,  $T_e$  was also mostly in  
284 the range of 3–7 s. Relatively higher  $T_e$  was found at B4, with most values  
285 between 4–7 s. In Aozaixia Bay (inner Daya Bay) represented by B3,  $T_e$  was

286 relatively small and mostly in the range 3–5 s, Similar values of  $T_e$  are found  
287 in Shenzhen Bay represented by B6. Moreover,  $T_e$  values greater than 10 s  
288 occasionally occurred at the 6 buoys, mostly due to the influence of tropical  
289 cyclones.

290 Based on  $H_s$  and  $T_e$ , the wave power,  $P$ , was estimated at the 6 buoy  
291 stations, Fig. 8. From comparison with time series of  $H_s$  shown in Fig. 7, the  
292 temporal variations of  $P$  and  $H_s$  were basically coherent, at both hourly, daily  
293 and monthly time scales. This can be explained from the relation of  $P$  and  
294  $H_s$ , since  $P$  is proportional to the square of  $H_s$ . For the period 2014–2016,  
295  $P$  was mostly confined to the range of  $10^2$  to  $10^3$   $\text{W m}^{-1}$  at B1, B4 and B5,  
296 while at B2, B3 and B6 wave power was considerably less, with values mostly  
297 less than  $100$   $\text{W m}^{-1}$ .

298 Statistics of annual wave climate at the six buoys were calculated and  
299 are summarized in Table 1, in terms of annual mean significant wave height  
300 and its standard deviation ( $(H_s)_{mean} \pm \text{std.dev.}$ ), maximum significant wave  
301 height ( $(H_s)_{max}$ ), annual mean wave period ( $(T_e)_{mean}$ ), and annual mean  
302 and maximum wave power (i.e.,  $P_{mean}$  and  $P_{max}$ ). It was not surprising that  
303  $(H_s)_{mean}$  averaged over the period 2014–2016 was very small, with values less  
304 than 0.5 m for the buoys except B4, and  $(H_s)_{mean}$  was only about 0.1 m at B3  
305 and B6. B4 displays a relatively  $(H_s)_{mean}$ , but was still very small (0.6 m).  
306 The largest  $(H_s)_{max}$  was found at B4, with value of over 4.0 m, occurring on  
307 September 16, 2014 when Typhoon Kalmaegi (No. 1415) passed through.  
308 For Inner Dapeng Bay, represented by B1 and B2,  $(H_s)_{max}$  was, respectively,  
309 2.5 m and 2.4 m, and about 1.7 m at B5. Smallest  $(H_s)_{max}$  was still found at  
310 B3 and B6 (less than 1 m).  $(T_e)_{mean}$  was relatively larger at B1, B2, B4 and

311 B5 (about 4.5 s), and smaller at B3 and B6 (3.5 s). The spatial distribution  
312 of wave power was similar to that of  $H_s$ : annual mean and maximum wave  
313 power,  $P_{mean}$  and  $P_{max}$ , were also largest at location B4 (1.25 kW m<sup>-1</sup> and  
314 88.1 kW m<sup>-1</sup>, respectively), followed by B5, B1, and B2 (respectively, 0.46,  
315 0.39, 0.26 kW m<sup>-1</sup> for  $P_{mean}$ ), while they were still smallest at B3 and B6  
316 (0.03 kW m<sup>-1</sup> for  $P_{mean}$ , and 1.2 and 1.6 kW m<sup>-1</sup> for  $P_{max}$ , respectively).

317 Monthly and seasonal wave climate variability are of importance for wave  
318 energy resource assessment. Monthly mean and seasonal characteristics of  
319  $H_s$  and  $T_e$  as well as  $P$  were thus investigated for the study region, based on  
320 the buoy observations over the period 2014–2016.

321 Fig. 9 shows the variability in monthly values of  $H_s$ ,  $T_e$  and  $P$  observed at  
322 the 6 buoy locations, while also displaying spatial difference in these variables  
323 between buoys. The monthly mean  $H_s$  for 2014–2016 can be briefly divided  
324 into three groups: smallest monthly mean  $H_s$  was found at B6 and B3, with  
325 values mostly less than 0.1 m; monthly mean values of  $H_s$  at B1, B2 and B5  
326 were mostly in the range of 0.2 m–0.5 m; largest monthly values  $H_s$  occurred  
327 at B5, which was between 0.5 m–0.8 m. Monthly mean values of  $T_e$  were also  
328 smallest at B3 and B6 (mostly around 3.5 s), followed by  $T_e$  at B5 (between  
329 4 s–5 s), while monthly  $T_e$  at B4, B2 and B1 were relatively large with values  
330 ranging between 4.5 s–6.0 s. Correspondingly, monthly mean wave power,  
331  $P$ , for the period 2014–2016 at the 6 locations can also be also divided into  
332 three groups by magnitude: largest at B4, with values ranging from about  
333 1 kW m<sup>-1</sup> to 3.5 kW m<sup>-1</sup>; monthly  $P$  were all less than 1 kW m<sup>-1</sup> at B1, B2  
334 and B5; while very small values were recorded at B3 and B6, with magnitudes  
335 of all less than 0.1 kW m<sup>-1</sup>.



336 Seasonal values of  $H_s$ ,  $T_e$  and  $P$  also displayed spatial variability be-  
337 tween the six buoy locations (see Fig. 9). At locations B3 and B6, seasonal  
338 variations in  $H_s$ ,  $T_e$  and  $P$  were very small and limited in 0.1 m, 4 s and  
339  $0.1 \text{ kW m}^{-1}$ , respectively. Seasonal differences in  $H_s$ ,  $T_e$  and  $P$  were evident  
340 at locations B1 and B5: seasonal values at B1 and B5 were relatively large  
341 in autumn and winter, and smaller in spring and summer months. Relative  
342 to B1 and B5, reversed seasonality was observed at B2, i.e., large values oc-  
343 curred in summer months with smaller values observed in winter. Largest  
344 seasonal values of  $H_s$  (around 0.6 m) were observed at B4, with relatively  
345 small variability. However, larger values of  $T_e$  and  $P$  were recorded in sum-  
346 mer and autumn months, with smaller values in winter and spring. From the  
347 comparison between seasonal and monthly winds (Fig. 5) and waves (Fig. 9),  
348 it is not surprising that the variability in the wind climate were not coherent  
349 with those of the wave climate in the study region, since, in general, waves  
350 in the coastal area might be not generated by local winds.

351 In addition to the numerical values of significant wave height and energy  
352 period, their frequency of occurrence is also important for assessment of  
353 wave energy resources. The combined scatter and energy diagrams, in terms  
354 of  $H_s$ ,  $T_e$ , and  $P$ , can provide convenient and comprehensive information  
355 for conveying the characteristics of wave energy resources. Fig. 10 shows the  
356 diagrams for the 6 sites, averaged at the same observational time (hourly) and  
357 all based on the data 2014–2016. In the figure, the significant wave height  
358 has been divided into intervals of one third of a meter in the range of 0–3 m,  
359 and the energy period has been divided into intervals of 1 s ranging from 1 s  
360 to 10 s. The colors on the diagrams show the proportion of incident energy

361 expected in one year, with numerical values given by the colour bar. The  
362 black curves, n the values of  $1 \text{ kW m}^{-1}$ ,  $3 \text{ kW m}^{-1}$ , and  $5 \text{ kW m}^{-1}$ , represent  
363 isolines of wave power calculated from Eq. 2. The numerical values on the  
364 diagrams in the figure represent the occurrence of a combination of  $H_s$  and  
365  $T_e$  within the corresponding range, in number of hours per year.

366 In Inner Dapeng bay, represented by buoys B1 and B2, Fig. 10 shows  
367 that, for buoy B1, sea states in the range of  $0.3\text{--}0.6 \text{ m}$  for  $H_s$  and  $5\text{--}6 \text{ s}$   
368 for  $T_e$  occurred most frequently, providing the largest contribution to the  
369 total annual wave energy (more than 30%), and the second largest contri-  
370 bution (about 18%) was from sea states with  $H_s$  between  $0.3\text{--}0.6 \text{ m}$  and  $T_e$   
371 between  $4\text{--}5 \text{ s}$ , which also displayed high frequency of occurrence; at B1, the  
372 frequency of occurrence of sea states with  $H_s$  between  $0 \text{ m}$  and  $0.3 \text{ m}$  and  
373  $T_e$  between  $4 \text{ s}$  and  $6 \text{ s}$  was also very high, while the contribution to the to-  
374 tal wave energy was less than 20%, since their values are relatively small;  
375 moreover, sea states of  $H_s$  between  $0.3 \text{ m}$  and  $0.6 \text{ m}$  and  $T_e$  between  $6 \text{ s}$  and  
376  $7 \text{ s}$  at B1 provided a relatively high contribution of about 15% to the wave  
377 energy, due to the relatively larger values in terms of  $H_s$  and  $T_e$ , even though  
378 their frequency of occurrence was relatively low; for buoy B2, sea states with  
379 highest frequency of occurrence were, respectively, in the range  $0.0\text{--}0.3 \text{ m}$   
380 for  $H_s$  and  $4\text{--}6 \text{ s}$  for  $T_e$ , and together they contributed more than 30% of  
381 total wave energy resources, while sea states of  $H_s$  between  $0.3\text{--}0.6 \text{ m}$  and  
382  $T_e$  between  $5\text{--}6 \text{ s}$  provided a significant contribution (more than 20%) to the  
383 wave energy resource, followed by the contribution from sea states of  $H_s$  and  
384  $T_e$ , respectively, in the range of  $0.3\text{--}0.6 \text{ m}$  and  $6\text{--}7 \text{ s}$ .

385 Concerning sea states, Fig. 10 clearly shows that for B3, located in Aoza-

386 ixia Bay, within Daya bay, almost all sea states were below 0.3 m and in  
387 the range 6–7 s, in terms of  $H_s$  and  $T_e$ , respectively, and contributing more  
388 than 60% of total wave energy resources there, with the second most signifi-  
389 cant contribution coming from sea states of  $H_s$  less than 0.3 m and  $T_e$  4 s to  
390 5 s. For the other buoy station in Daya Bay, B5, sea states with the high-  
391 est frequency of occurrence were in the range 0.0–0.3 m and 4–5 s for  $H_s$   
392 and  $T_e$ , respectively, providing the largest contribution to the total annual  
393 wave energy (more than 43%); with the second largest contribution (about  
394 30%) coming from sea states with  $H_s$  and  $T_e$  between 0–0.3 m and 5–6 s,  
395 respectively; the frequency of occurrence of sea states with  $H_s$  below 0.3 m  
396 were also significantly high, but their contribution to the total annual energy  
397 resources was relatively small.

398 For buoy B4, located off the coast of Dapeng peninsula and in the deepest  
399 location of the 6 buoys, sea states in the range of 0.3–0.9 m for  $H_s$  and 4–6 s  
400 for  $T_e$  provided the largest contribution to the total annual wave energy (all  
401 together more than 70%), while sea states with larger  $H_s$ , between 0.9–1.2 m,  
402 and  $T_e$  between 5–6 s contributed about 8% of total wave energy resources.  
403 For B6, located in the narrow Shenzhen Bay, sea states in terms of  $H_s$  and  
404  $T_e$ , and their contributions to total wave energy, were similar to those at  
405 location B3, where water depth is also very shallow as well.

406 Overall, for all buoys, most sea states in terms of  $H_s$  were below 0.6 m.,  
407 Concerning  $T_e$ , most sea state values were between 4–6 s for B1–B2, and  
408 B4–B5, while values of between 3–4 s were found for B3 and B6. A basic  
409 knowledge of significant wave height values informs that values below 0.6 m  
410 in the ocean are quite small. It is not surprising that  $H_s$  is small in the

411 study region, since water depths are correspondingly low and the region is  
412 relatively closed off from open seas.

413 Wave direction plays an important role in wave energy assessment. Fig. 11  
414 shows seasonal distributions of incoming wave direction for the 6 buoys in  
415 the study region. It is apparent from this figure that there was no obvious  
416 seasonal change in wave direction for the 6 buoys. Wave directions at these  
417 buoys locations were not in accordance with the corresponding wind direc-  
418 tions (see Fig. 6), but they mainly reflected the wave propagating directions  
419 of propagating away from generation sources in the open region towards the  
420 coast, so that none at all was from the IV quadrant due to the coastline  
421 orientations at the buoys. Moreover, in all directions wave power was mostly  
422 less than  $1 \text{ kW m}^{-1}$ .

423 In Dapeng bay, most waves came from the II quadrant: for B1, the pre-  
424 vailing wave direction was from the SE, with a very minor contribution from  
425 the SSE; for B2, southerly waves prevail in all seasons except in Winter, fol-  
426 lowed by SSW, whereas SSW waves a little more occurred in winter, with a  
427 little lower occurrence (about 31%) from the south. For Daya bay, at B3,  
428 most of the wave energy was provided by waves from the I quadrant, and  
429 the prevailing wave direction was NE, followed by ENE and NNE, which did  
430 not match the prevailing wind direction (see Fig. 6). This indicates that  
431 the waves at B3 were mostly not generated by local winds, but mostly came  
432 from the open region where the waves propagated to the coast. As for the  
433 other buoy in Daya bay, B5, most of the wave energy was contributed by  
434 easterly waves: ESE waves prevailed in winter and autumn, followed by N,  
435 whereas northerly waves occurred more in Spring and summer, followed by

436 ESE; a minor contribution (less than 5%) was due to waves from the ENE.  
437 At B4, Fig. 6 reveals that most waves came from the II quadrant, which  
438 did not match the prevailing wind directions, indicating that the waves were  
439 not generated by local winds, but from waves propagating away from gen-  
440 eration sources in the open region. For B6 located in Shenzhen Bay, most  
441 of the waves (more than 50% on average for the all seasons) came from III,  
442 as expected, with southwesterly and WSW directions prevailing. However,  
443 it is noted that occurrence from other directions was rare, especially from  
444 the opposite direction, i.e., NE and ENE, which might be due to the fact  
445 that this is a relatively narrow area, and where the influence of reflected and  
446 refracted waves might be of more significance.

447 Previous studies have shown that waves transport energy supplied to  
448 them over vast distances, and dissipative effects may play only a smaller role  
449 in deep water, as opposed to the surf zone; nearshore waves are nonlinearly  
450 related to the strength, fetch, and duration of the wind [62]. Therefore, the  
451 local wave climate can be frequently affected by strong incident waves or  
452 wind fetch both inside and outside the study region.

453 Last but not least, we provide a brief discussion concerning the relation-  
454 ship between the wind energy and the wave climate for the study area. Fig. 12  
455 displays a preliminary correlation between the wind speed/energy and the  
456 wave climate based on the local buoy measurements. Results from all buoys  
457 other than B5 (not recorded) are displayed. The upper panels of Fig. 12 show  
458 the relationship between anomalies of monthly averaged data (monthly val-  
459 ues minus monthly climatology) of wind speed and significant wave height for  
460 the period 2014–2016. For this long-timescale (low frequency) comparison,

461 the threshold correlation coefficient at the 95% and 99% significance levels  
462 is about 0.35 and 0.45, respectively (the sample of the time series of the  
463 monthly anomalies is about 30). It can be seen from this figure that, except  
464 at B3 buoy location, all other locations display a relatively small correla-  
465 tion between wind strength and wave conditions. Moreover, we attempted  
466 to calculate the delay/forward correlations, but they are still insignificant  
467 (not shown). The bottom panel in Fig. 12 describes correlations between  
468 daily anomalies (daily values minus monthly climatology) of wind speed and  
469  $H_s$  for the period 2014–2016. The coefficients were all statistically signifi-  
470 cant (sample numbers for the time series are all greater than 550, and the  
471 threshold correlation coefficient at the 95% and 99% significance levels is less  
472 than 0.11). At Dapeng Bay, represented by buoys B1 and B2, correlations  
473 were over 0.3 for the period 2014–2016. At B3, located in Daya Bay, the  
474 correlation was very high, 0.77. A relatively high correlation is also found at  
475 station B4 (0.60). For Shenzhen Bay (B6), the correlation coefficient is about  
476 0.39, similar to values for Dapeng Bay. Therefore, at this daily timescale, the  
477 local wind energy significantly influences the wave climate in the study area.  
478 Thus, care must be taken before we can conclude whether the wave climate in  
479 the study region might be more affected by the local wind at daily timescale  
480 rather than for long-time statistics when non-local wave signals from outside  
481 the study region get more involved.

#### 482 **4. Summary and Conclusions**

483 In this study, wind and wave climates for the Shenzhen coastal region are  
484 evaluated by means of buoy observational data. Buoys were first placed in

485 the region by the city local government in 2014 to observe and monitor the  
486 atmospheric and hydrodynamic climate of the region. Six buoys are located  
487 in different areas of the study region, including Dapeng Bay, Daya Bay,  
488 Shenzhen Bay, and the area off the tip of the Dapeng peninsula. The waters  
489 in these areas are very shallow, ranging in depth from about 3 m–22 m.

490 In terms of wind speed and direction at the buoys (2.5 m above the sea  
491 surface), wind climate and potential wind energy resources were assessed in  
492 detail for the period 2014–2016. It was found that the annual mean wind  
493 speed at the buoy locations for the period 2014–2016 varied from about  
494  $3.1 \text{ m s}^{-1}$  to  $4.1 \text{ m s}^{-1}$ , with maximum wind speeds of more than  $17 \text{ m s}^{-1}$  oc-  
495 ccurring as a result of tropical cyclones. These winds resulted in annual mean  
496 wind powers of about  $37\text{--}94 \text{ W m}^{-2}$ . Among the buoys, largest averaged  
497 wind speed and power were found at B4, located in the relatively open area  
498 off the southern coast of Dapeng peninsula. On average, more than 80% of  
499 wind speeds were less than  $5 \text{ m s}^{-1}$  in the study region. However, the wind  
500 speed was relatively large at location B4, where about 45% of wind speeds  
501 were over  $5 \text{ m s}^{-1}$  in winter and autumn, and 20% in summer and spring.

502 Seasonal variability in wind speed and power fluctuated at the different  
503 buoy locations over the 2014–2016 period. At B1 and B4, seasonal variability  
504 was relatively large in autumn and winter, and smaller in spring and summer  
505 months. However, reversed seasonality occurred at location B6, where wind  
506 and wind power were relatively large in spring and summer, and were smaller  
507 in autumn and winter. Seasonal variations were relatively small at B2 and  
508 B3 locations.

509 Seasonal and spatial wind direction variability differed between buoys

510 B1–B4 (no wind direction data at B5 and B6). At B1, located in the north-  
511 west end of Dapeng Bay, the prevailing wind direction in winter, spring, sum-  
512 mer and autumn was, respectively, easterly, easterly to southerly, southerly,  
513 and southerly. The prevailing wind direction was from the east in all seasons  
514 at location B2. At B3, located in Daya Bay, the largest contribution to wind  
515 energy resources was provided by the southerly winds, in all seasons, with  
516 SSE and SSW winds also providing considerable contributions. The prevail-  
517 ing wind direction at B4 varied seasonally, with occurrence of less than 15%  
518 from any particular direction: in winter, most winds were from the the I  
519 quadrant, followed by the II quadrant; westerly winds prevailed in spring,  
520 with southerly winds prevailing in autumn.

521 Wave climate and potential wave energy resources in terms of wave height,  
522 wave energy period, wave direction, and wave power were also evaluated for  
523 the period 2014–2016. The data showed that at the 6 buoy locations,  $H_s$  was  
524 mostly less than 1 m, and even less than 0.5 m at B2, B3, and B6 locations.  
525 As a result, wave power,  $P$ , was mostly limited to the range  $10^2$  to  $10^3$   $\text{W m}^{-1}$   
526 at B1, B4 and B5, and mostly less than  $100$   $\text{W m}^{-1}$  at the other locations.  
527 This may be due to the facts that, first, water depth is very shallow, and,  
528 secondly, the buoys are located in bays where the sea is somewhat semi-  
529 enclosed, all of which are not favorable for the development of wind waves.  
530  $T_e$  was mostly in the range of 3–7 s in the study region, with values of more  
531 than 10 s occasionally occurring at all 6 buoys, mostly during periods of  
532 tropical cyclones.

533 It was not surprising that annual mean significant wave height,  $(H_s)_{mean}$ ,  
534 for the period 2014–2016 was relatively small, with values of less than 1.0 m



535 for the study region, and largest values of ( $H_s$ ) found at B4 of over 4.0 m.  
536 In addition, most sea states in terms of  $H_s$  were less than 0.6 m, with  $T_e$   
537 between 4–6 s for B1–B2, and B4–B5, and 3–4 s for B3 and B6. The  
538 annual mean wave energy period,  $(T_e)_{mean}$ , was relatively large at B1, B2,  
539 B4 and B5 (about 4.5 s), and smaller at B3 and B6 (3.5 s). Correspondingly,  
540 the annual mean wave power was largest at B4 ( $1.25 \text{ kW m}^{-1}$ ), and between  
541  $0.26\text{--}0.46 \text{ kW m}^{-1}$  at B1, B2, and B5, and smallest at B3 and B6, with values  
542 of only  $0.03 \text{ kW m}^{-1}$ . Therefore, we can conclude that the potential of the  
543 wave energy resource at the buoy locations are very small.

#### 544 **Acknowledgements**

545 X. Chen was funded by the National Natural Science Foundation of China  
546 (NSFC) grant 41506042. Y. Zhang was funded by the NSFC grant 51609043  
547 and by Key Laboratory of Coastal Disaster and Defense, Ministry of Educa-  
548 tion, China, under the award 2016001.

549 **References**

- 550 [1] China's Action Plan on Prevention and Control of Air Pollution. the  
551 State Council of the People's Republic of China; 2013.
- 552 [2] REN21. RENEWABLES 2015: Global Status Report (the Renewable  
553 Energy Policy Network for the 21st Century). REN21; 2015.
- 554 [3] Atlas of UK Marine Renewable Energy Resources. Technical Report,  
555 Report No.1432; 2008.
- 556 [4] Higgins P, Foley A. The evolution of offshore wind power in the United  
557 Kingdom. *Renewable and Sustainable Energy Reviews* 2014;37:599–612.
- 558 [5] Mollison D, Pontes MT. Assessing the Portuguese wave-power resource.  
559 *Energy* 1992;17(3):255–68.
- 560 [6] Rusu E, Guedes Soares C. Numerical modelling to estimate the spatial  
561 distribution of the wave energy in the Portuguese nearshore. *Renewable*  
562 *Energy* 2009;34(6):1501–16.
- 563 [7] Mota P, Pinto JP. Wave energy potential along the western Portuguese  
564 coast. *Renewable Energy* 2014;71:8–17.
- 565 [8] Waters R, Engström J, Isberg J, Leijon M. Wave climate off the Swedish  
566 west coast. *Renewable Energy* 2009;34(6):1600–6.
- 567 [9] Beels C, De Rouck J, Verhaeghe H, Geeraerts J, Dumon G. Wave energy  
568 on the Belgian continental shelf. In: *Oceans 2007-Europe*. IEEE; 2007.  
569 p. 1–6.

- 570 [10] Iglesias G, López M, Carballo R, Castro A, Fraguera JA, Frigaard  
571 P. Wave energy potential in Galicia (NW Spain). *Renewable Energy*  
572 2009;34(11):2323–33.
- 573 [11] Iglesias G, Carballo R. Wave energy resource in the Estaca de Bares  
574 area (Spain). *Renewable Energy* 2010;35(7):1574–84.
- 575 [12] Iglesias G, Carballo R. Offshore and inshore wave energy assessment:  
576 Asturias (N Spain). *Energy* 2010;35(5):1964–72.
- 577 [13] López-Ruiz A, Bergillos RJ, Ortega-Sánchez M. The importance of wave  
578 climate forecasting on the decision-making process for nearshore wave  
579 energy exploitation. *Applied Energy* 2016;182:191–203.
- 580 [14] Foley AM, Kerlin C, Leahy PG. Offshore wind resource estimation using  
581 wave buoy data; 2012. p. 1114–19.
- 582 [15] Gallagher S, Tiron R, Whelan E, Gleeson E, Dias F, McGrath R. The  
583 nearshore wind and wave energy potential of Ireland: A high reso-  
584 lution assessment of availability and accessibility. *Renewable Energy*  
585 2016;88:494–516.
- 586 [16] Clément A, McCullen P, Falcão A, Fiorentino A, Gardner F, Hammar-  
587 lund K, et al. Wave energy in Europe: current status and perspectives.  
588 *Renewable and Sustainable Energy Reviews* 2002;6(5):405–31.
- 589 [17] Henfridsson U, Neimane V, Strand K, Kapper R, Bernhoff H, Danielsson  
590 O, et al. Wave energy potential in the Baltic Sea and the Danish part  
591 of the North Sea, with reflections on the Skagerrak. *Renewable Energy*  
592 2007;32(12):2069–84.

- 593 [18] Akpınar A, Komurcu MI. Assessment of wave energy resource of the  
594 Black sea based on 15-year numerical hindcast data. *Applied Energy*  
595 2013;101:502–12.
- 596 [19] Langodan S, Viswanadhapalli Y, Dasari HP, and Ibrahim Hoteit OK. A  
597 high-resolution assessment of wind and wave energy potentials in the  
598 Red Sea. *Applied Energy* 2016;181:244–55.
- 599 [20] Appendini CM, Urbano-Latorre CP, Figueroa B, Dagua-Paz CJ, Torres-  
600 Freyermuth A, Salles P. Wave energy potential assessment in the  
601 Caribbean Low Level Jet using wave hindcast information. *Applied*  
602 *Energy* 2015;137:375–84.
- 603 [21] Hughes MG, Heap AD. National-scale wave energy resource assessment  
604 for Australia. *Renewable Energy* 2010;35(8):1783–91.
- 605 [22] Morim J, Cartwright N, Etemad-Shahidi A, Strauss D, Hemer M. Wave  
606 energy resource assessment along the Southeast coast of Australia on  
607 the basis of a 31-year hindcast. *Applied Energy* 2016;184:276–97.
- 608 [23] Cornett AM. Inventory of Canada’s offshore wave energy resources.  
609 In: 25th International Conference on Offshore Mechanics and Arctic  
610 Engineering. American Society of Mechanical Engineers; 2006. p. 353–  
611 62.
- 612 [24] Abbaspour M, Rahimi R. Iran atlas of offshore renewable energies.  
613 *Renewable Energy* 2011;36:388–398.
- 614 [25] Baba M. Wave power potential off the south-west Indian coast. *Energy*  
615 1987;12(6):501–7.

- 616 [26] Sivaramakrishnan TR. Wave power over the Indian seas during the  
617 southwest monsoon season. *Energy* 1992;17(6):625–7.
- 618 [27] Kumar VS, Dubhashi KK, Nair TMB, Singh J. Wave power potential at  
619 few shallow water locations around Indian coast. *Current Science India*  
620 2013;104(9):1219–24.
- 621 [28] Kumar VS, Anoop TR. Wave energy resource assessment for the Indian  
622 shelf seas. *Renewable Energy* 2015;76:212–219.
- 623 [29] Gadad S, Deka PC. Offshore wind power resource assessment using  
624 Oceansat-2 scatterometer data at a regional scale. *Applied Energy*  
625 2016;176:157–70.
- 626 [30] Oh KY, Kim JY, Lee JK, Ryu MS, Lee JS. An assessment of wind energy  
627 potential at the demonstration offshore wind farm in Korea. *Energy*  
628 2012;46:555–63.
- 629 [31] Karthikeya BR, Negi PS, Srikanth N. Wind resource assessment for  
630 urban renewable energy application in Singapore. *Renewable Energy*  
631 2016;87:403–14.
- 632 [32] Watts D, Oses N, Pérez R. Assessment of wind energy potential in Chile:  
633 A project-based regional wind supply function approach. *Renewable*  
634 *Energy* 2016;96:738–55.
- 635 [33] Hagerman G. Wave Energy resource and economic Assessment for the  
636 State of Hawaii. Prepared by SEASUN Power Systems for the Depart-  
637 ment of Business, Economic Development, and Tourism, Final Report;  
638 1992.

- 639 [34] Stopa JE, Filipot JF, Li N, Cheung KF, Chen YL, Vega L. Wave  
640 energy resources along the Hawaiian Island chain. *Renewable Energy*  
641 2013;55:305–321.
- 642 [35] Hagerman G. Southern New England wave energy resource potential.  
643 *Proc. Building Energy 2001, Boston, USA; 2001.*
- 644 [36] Beyene A, Wilson JH. Comparison of wave energy flux for northern,  
645 central, and southern coast of California based on long-term statistical  
646 wave data. *Energy* 2006;31(12):1856–69.
- 647 [37] Wilson JH, Beyene A. California wave energy resource evaluation. *Jour-*  
648 *nal of Coastal Research* 2007;p. 679–90.
- 649 [38] Defne Z, Haas KA, Fritz HM. Wave power potential along the Atlantic  
650 coast of the southeastern USA. *Renewable Energy* 2009;34(10):2197–  
651 205.
- 652 [39] Lenee-Bluhm P, Paasch R, Özkan-Haller H. Characterizing the wave  
653 energy resource of the US Pacific Northwest. *Renewable Energy*  
654 2011;36(8):2106–19.
- 655 [40] Cornett AM, et al. A global wave energy resource assessment. In: *Pro-*  
656 *ceedings of the Eighteenth International Offshore and Polar Engineering*  
657 *Conference, Vancouver, Canada; 2008. p. 1–9.*
- 658 [41] Mork G, Barstow S, Kabuth A, Pontes MT. Assessing the global wave  
659 energy potential. In: *ASME 2010 29th International Conference on*  
660 *Ocean, Offshore and Arctic Engineering. American Society of Mechan-*  
661 *ical Engineers; 2010. p. 447–54.*

- 662 [42] Gunn K, Stock-Williams C. Quantifying the global wave power resource.  
663 Renewable Energy 2012;44:296–304.
- 664 [43] Arinaga RA, Cheung KF. Atlas of global wave energy from 10 years of  
665 reanalysis and hindcast data. Renewable Energy 2012;39:49–64.
- 666 [44] Reguero BG, Losada IJ, Méndez FJ. A global wave power resource  
667 and its seasonal, interannual and long-term variability. Applied Energy  
668 2015;148:366–80.
- 669 [45] Zhou W, Yang H, Fang Z. Wind power potential and characteristic  
670 analysis of the Pearl River Delta region, China. Renewable Energy  
671 ;31(6).
- 672 [46] Li J, Gao H, Shi P, Shi J, Ma L, Qin H. China wind power report 2007;  
673 2007.
- 674 [47] Zhang D, Li W, Lin Y. Wave energy in China: Current status and  
675 perspectives. Renewable energy 2009;34(10):2089–92.
- 676 [48] Xia C, Song Z. Wind energy in China: current scenario and future  
677 perspectives. Renewable and Sustainable Energy Reviews 2009;13:1966–  
678 74.
- 679 [49] Han J, Arthur PJM, Lu Y, Zhang L. Onshore wind power develop-  
680 ment in China: challenges behind a successful story. Energy Policy  
681 2009;37:2941–51.
- 682 [50] Rajgor G. China gets serious on offshore wind. Renewable Energy Focus  
683 2010;September/October.

- 684 [51] Wang S, Yuan P, Li D, Jiao Y. An overview of ocean renewable energy in  
685 China. *Renewable and Sustainable Energy Reviews* 2011;15(1):91–111.
- 686 [52] Zheng C, Zhuang H, Li X, Li X. Wind energy and wave energy resources  
687 assessment in the East China Sea and South China Sea. *Science China  
688 Technological Sciences* 2012;55(1):163–73.
- 689 [53] Jiang D, Zhuang D, Huang Y, Wang J, Fu J. Evaluating the spatio-  
690 temporal variation of China’s offshore wind resources based on remotely  
691 sensed wind field data. *Renewable and Sustainable Energy Reviews*  
692 2013;24:142–148.
- 693 [54] Wu S, Liu C, Chen X. Offshore wave energy resource assessment in the  
694 East China Sea. *Renewable Energy* 2015;76:628–36.
- 695 [55] Li G. Feasibility of large scale offshore wind power for Hong Kong a  
696 preliminary study. *Renewable Energy* 2000;21(3):387–402.
- 697 [56] Lu L, Yang H, Burnett J. Investigation on wind power potential on  
698 Hong Kong islands a  
699 an analysis of wind power and wind turbine characteristics. *Renewable Energy* 2002;27(1):1–12.
- 700 [57] Gao X, Yang H, Lu L. Study on offshore wind power potential and wind  
701 farm optimization in Hong Kong. *Energy* 2014;130:519–31.
- 702 [58] Shu ZR, Li QS, Chan PW. Investigation of offshore wind energy po-  
703 tential in Hong Kong based on Weibull distribution function. *Applied  
704 Energy* 2015;156:362–73.



- 705 [59] Roger B. Wave energy forecasting accuracy as a function of forecast time  
706 horizon; 2009.
- 707 [60] Committee CSA. Classification of tropical cyclones (GB/T19201-2006);  
708 2006.
- 709 [61] Ying M, Zhang W, Yu H, Lu X, Feng J, Fan Y, et al. An Overview  
710 of the China Meteorological Administration Tropical Cyclone Database.  
711 Journal of Atmospheric and Oceanic Technology 2013;(2013).
- 712 [62] Zhang Y, Kennedy AB, Tomiczek T, Donahue AS, Westerink JJ. Val-  
713 idation of Boussinesq-Green-Naghdi Modelling for Surf Zone Hydrody-  
714 namics. Ocean Engineering 2016;111:299–309.

Table 1: List of measurement buoys in the Shenzhen coastal region with water depth and some fundamental mean wind and wave characteristics. The collected buoy data covered from April 2014 to the end of 2016, with data gap that can be seen in Fig. 2. Main wind and wave characteristics were statistically calculated, including wind speed,  $V$  ( $\text{m s}^{-1}$ ); wind power,  $W$  ( $\text{W m}^{-2}$ ); significant wave height,  $H_s$  (m); wave energy period,  $T_e$  (s); wave power,  $P$  ( $\text{kW m}^{-1}$ ).

Buoy	Depth (m)	$V_{mean}$ $\pm$ std.dev.	$V_{max}$	$W_{mean}$	$W_{max}$	$(H_s)_{mean}$ $\pm$ std.dev.	$(H_s)_{max}$	$(T_e)_{mean}$	$P_{mean}$	$P_{max}$
B1	11	$3.1 \pm 2.3$	17.5	58	3282	$0.34 \pm 0.18$	2.5	4.7	0.39	22.5
B2	11	$3.1 \pm 1.7$	17.6	37	3339	$0.25 \pm 0.17$	2.4	4.7	0.26	28.0
B3	5	$3.4 \pm 2.0$	15.6	52	2325	$0.11 \pm 0.05$	0.8	3.5	0.03	1.2
B4	22	$4.1 \pm 2.5$	17.1	94	3063	$0.62 \pm 0.30$	4.3	4.5	1.25	88.1
B5	12	/	/	/	/	$0.38 \pm 0.23$	1.7	4.3	0.46	8.7
B6	3	$3.6 \pm 1.8$	15.7	51	2347	$0.13 \pm 0.05$	0.9	3.5	0.03	1.6

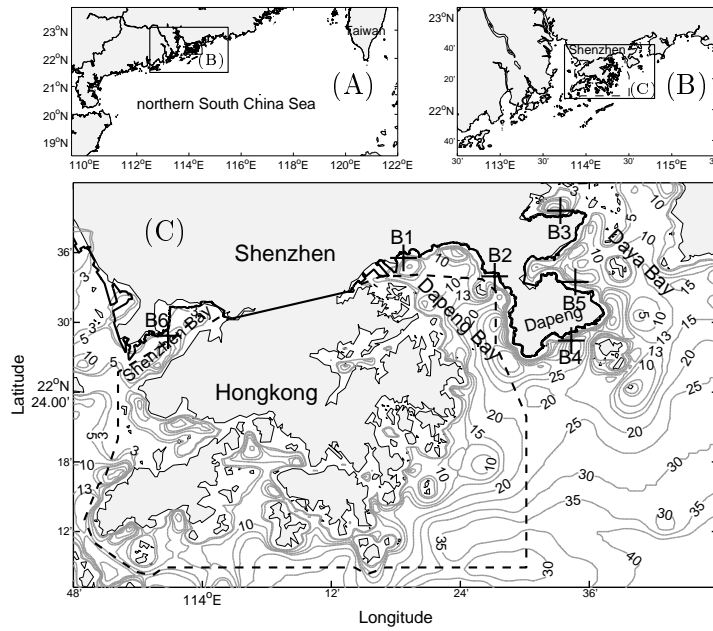


Figure 1: (C): Bathymetry contours (m) for the study area together with locations of the six wind and wave measurement buoys (B1-B6) in the coastal Shenzhen region (bottom/main panel). The study area is situated in the northern South China Sea (top panels). The broken line represents the boundary of Hong Kong waters.

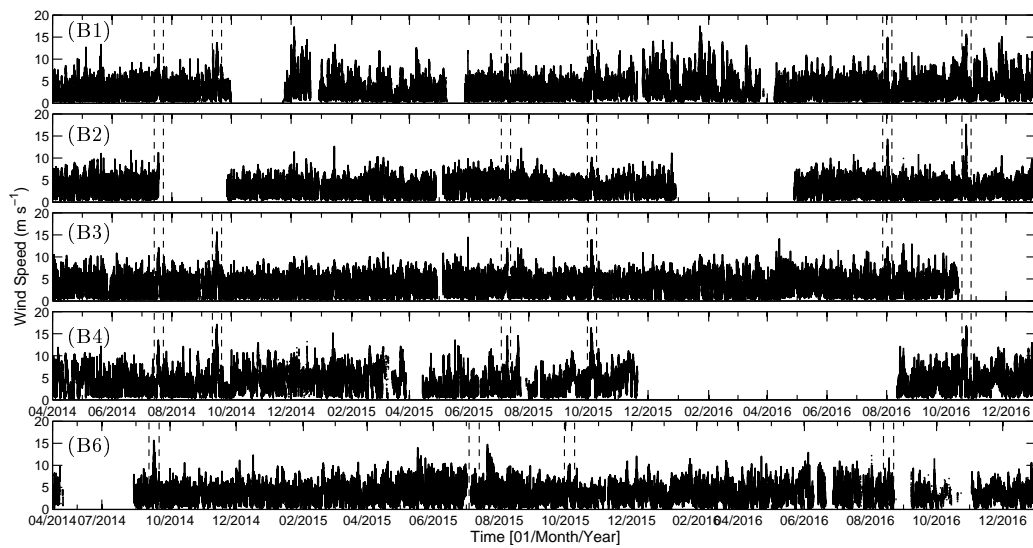


Figure 2: Time series of wind speed ( $\text{m s}^{-1}$ ) at the buoy locations (B1–B4 and B6) shown in Fig. 1 for the period 2014–2016. Dashed lines show the time periods of the tropical cyclones (see Fig. 4) passing through the study region. Wind data were missed at B5 buoy.

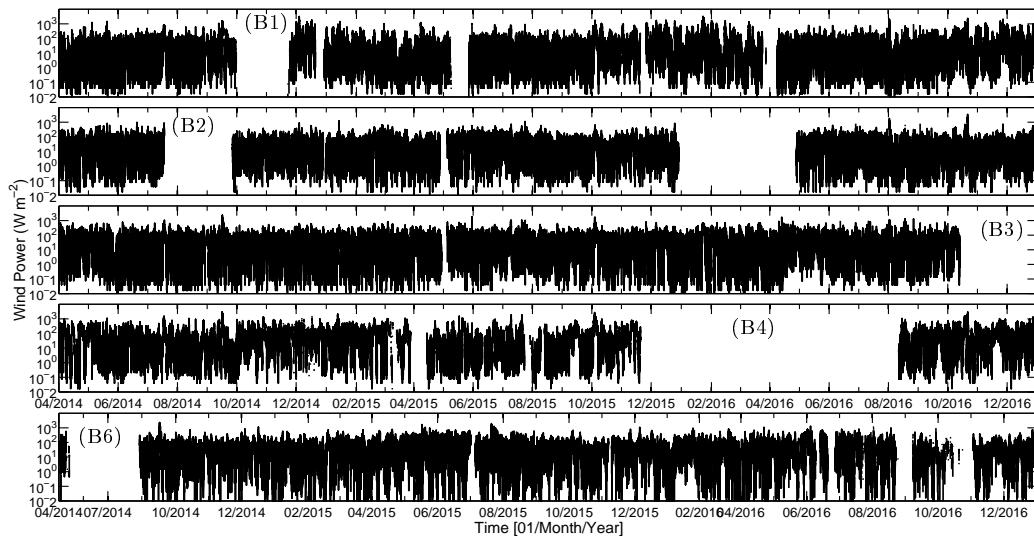


Figure 3: Time series of wind power ( $\text{W m}^{-2}$ ) at locations B1–B4 and B6 shown in Fig. 1 for the period 2014–2016.

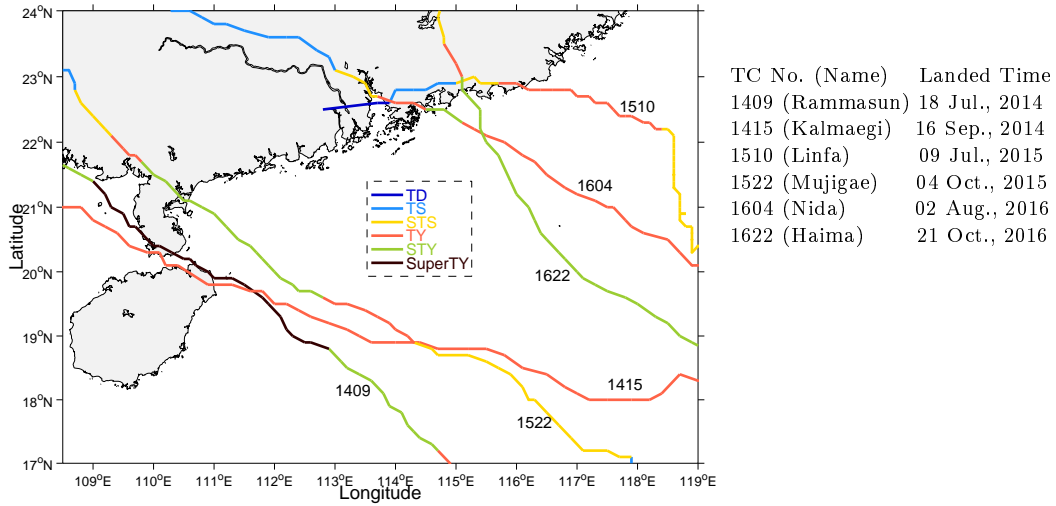


Figure 4: Left: Paths of tropical cyclones (TCs) passing through the northern South China Sea for the period 2014–2016. Right: The TC No. (Name) and landed time. Data source: [http://tcdata.typhoon.gov.cn/zj1jsjj\\_sm.html](http://tcdata.typhoon.gov.cn/zj1jsjj_sm.html) [61]. The classifications of the TCs in China are as follows: Tropical Depression (TD;  $10.8\text{--}17.1\text{ m s}^{-1}$ ); Tropical Storm (TS;  $17.2\text{--}24.4\text{ m s}^{-1}$ ); Severe Tropical Storm (STS;  $24.5\text{--}32.6\text{ m s}^{-1}$ ); TYphoon (TY;  $32.7\text{--}41.4\text{ m s}^{-1}$ ); Severe TYphoon (STY;  $41.5\text{--}50.9\text{ m s}^{-1}$ ); and Super TYphoon (SuperTY;  $\geq 51.0\text{ m s}^{-1}$ )

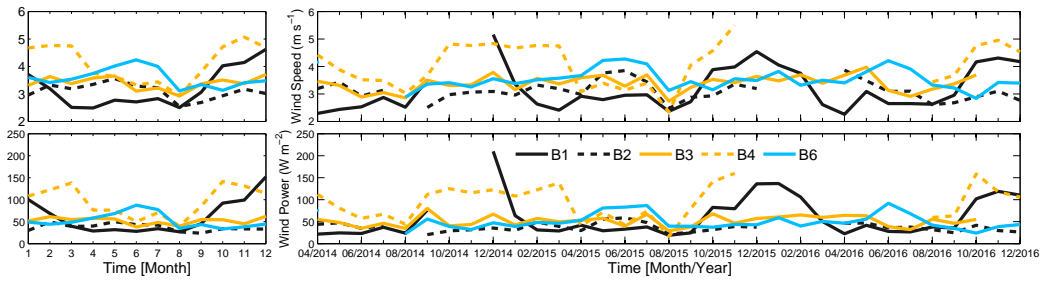


Figure 5: Seasonal (left) and monthly (right) mean wind speed ( $\text{m s}^{-1}$ ) and wind power ( $\text{W m}^{-2}$ ) for the buoys B1–B4 and B6 shown in Fig. 1.

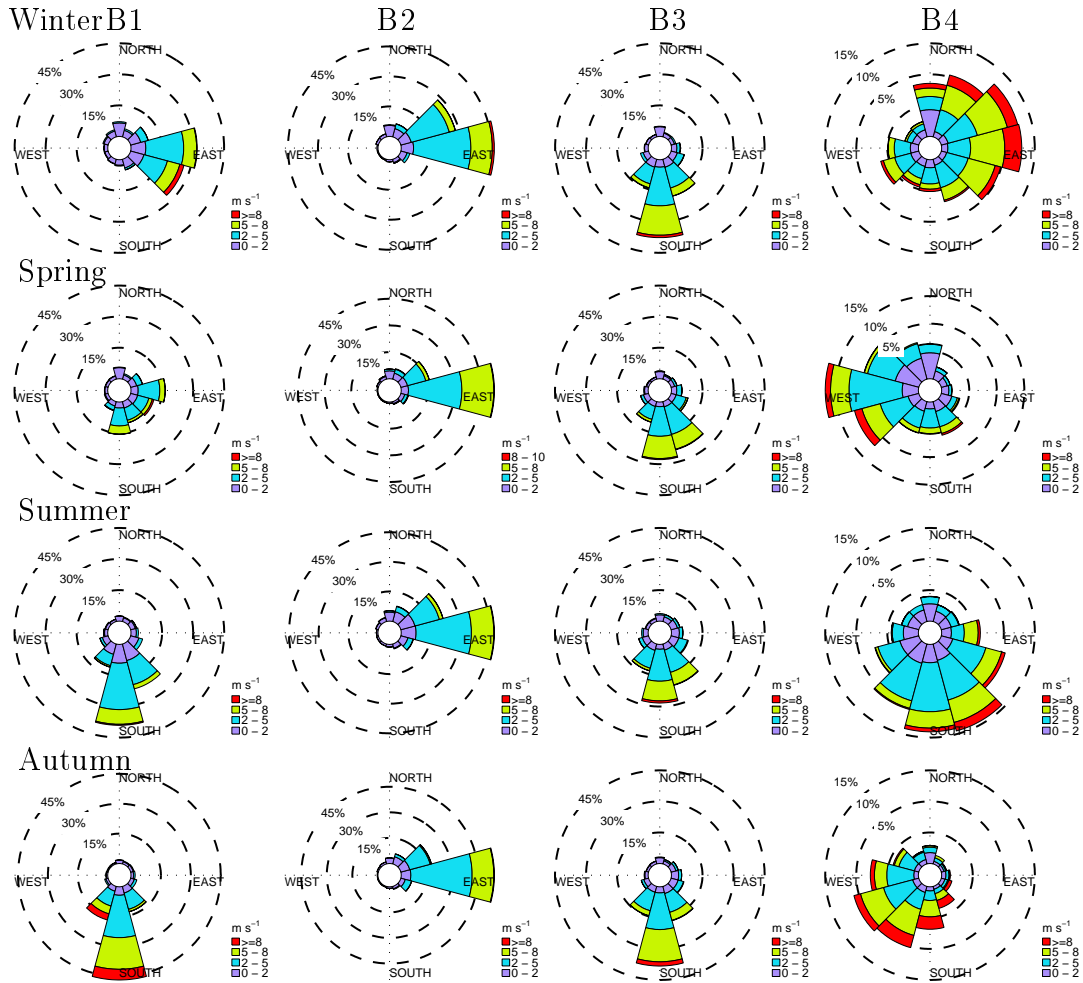


Figure 6: Seasonal wind speed and direction roses based on the measurement from buoys B1–B4 for the period 2014–2016. Wind direction data were missed at B5 and B6 locations.

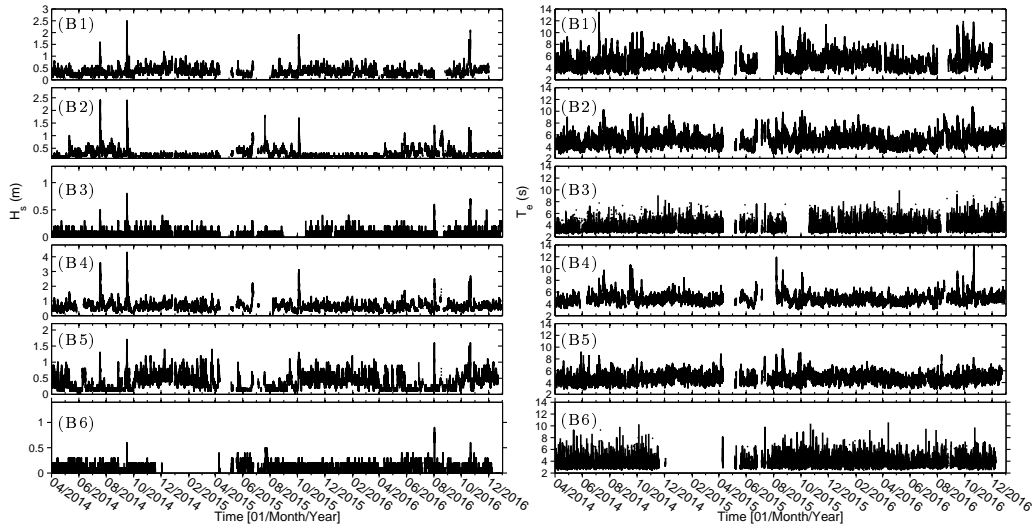


Figure 7: Time series of significant wave heights ( $H_s$  in m) and wave energy periods ( $T_e$  in s) at the six buoy locations (B1–B6) for the period 2014–2016.

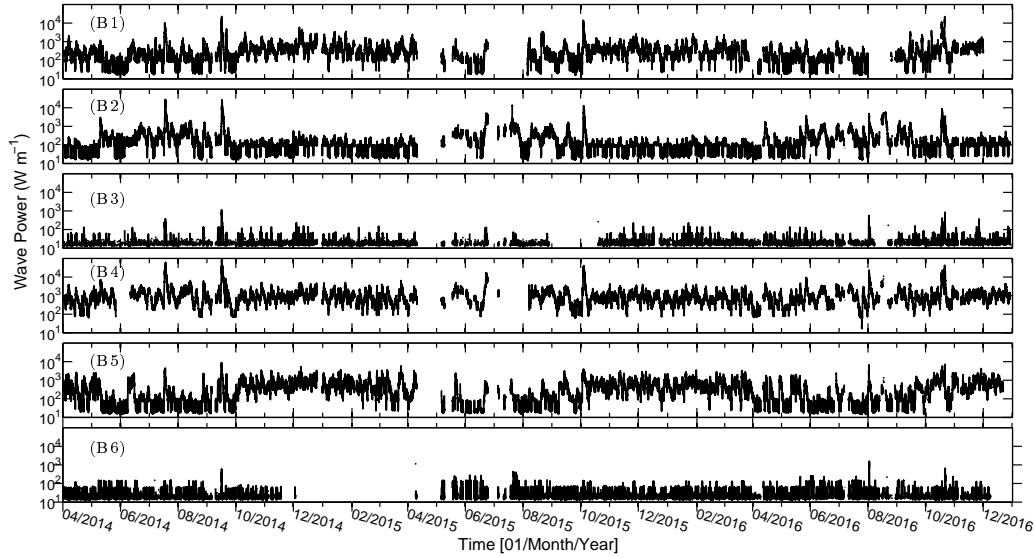


Figure 8: Time series of wave power ( $\text{W m}^{-1}$ ),  $P$ , at buoy locations of B1–B6 shown in Fig. 1 for the period 2014–2016.



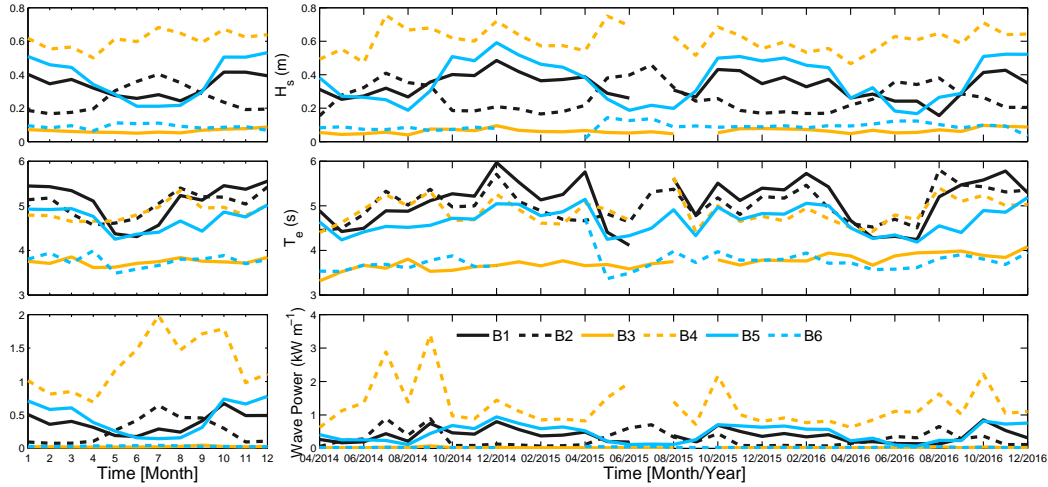


Figure 9: Seasonal (left) and monthly (right) mean significant wave height ( $H_s$ ), energy period ( $T_e$ ), and wave power ( $P$ ), for the six buoys (B1–B6) shown in Fig. 1 for the period 2014–2016.

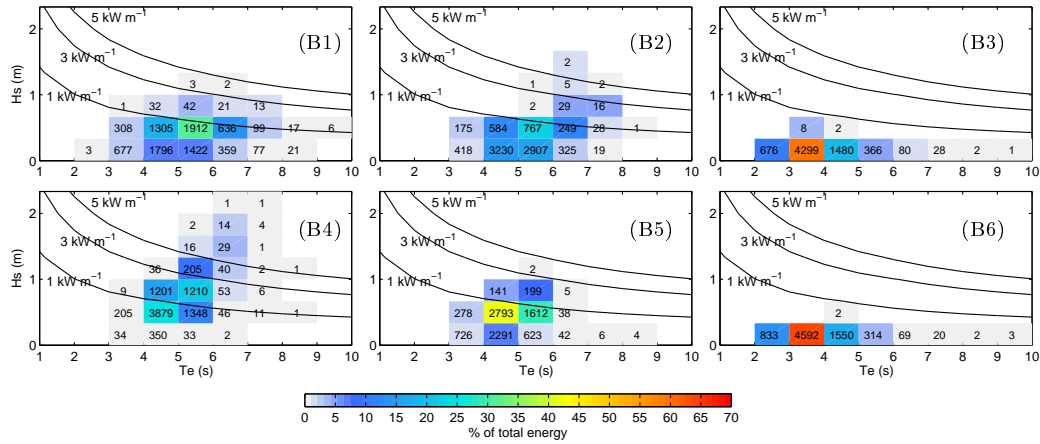


Figure 10: Bivariate distributions of occurrence and energy in terms of significant wave height ( $H_s$ ), and energy period ( $T_e$ ) averaged for the period 2014–2016 for at the six stations displayed in Fig. 1. The color scale, as a percentage, represents the contribution of the sea state to the total energy, while the black numbers indicates the occurrence of sea states in number of hours in one year.

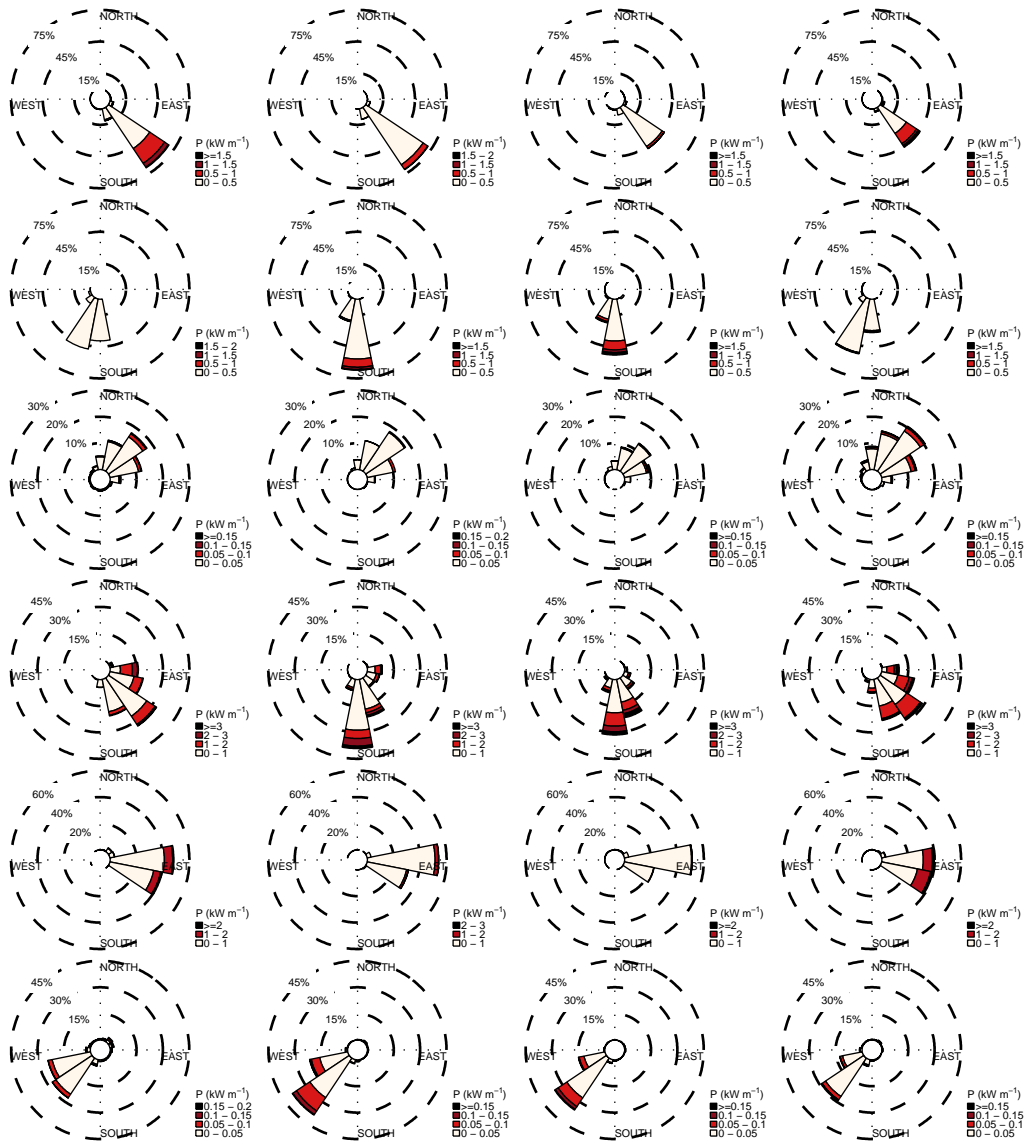


Figure 11: Seasonal wave power and direction roses based on the measurement from the buoys B1–B6 for the period 2014–2016.

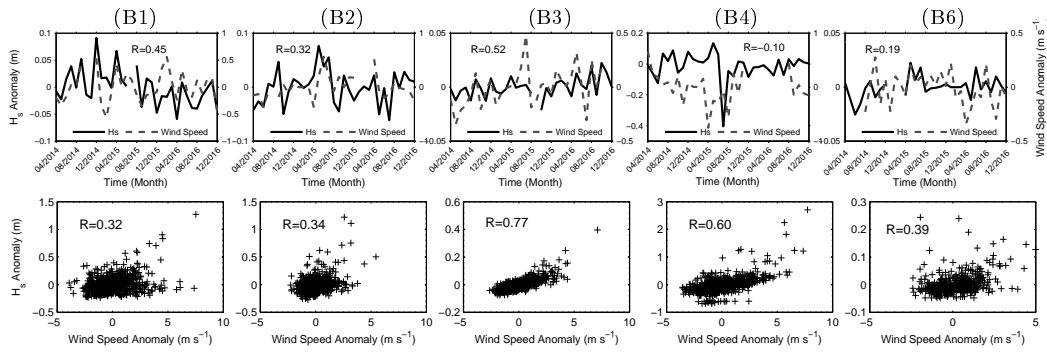


Figure 12: Top panel: the relationship between anomalies of monthly averaged data (monthly values minus monthly climatology) of wind speed and significant wave height,  $H_s$ , at buoys B1–B4 and B6 for the period 2014–2016. Bottom panel: the relationship between anomalies of daily averaged (daily values minus monthly climatology) of wind speed and  $H_s$  at the buoys B1–B4 and B6 (as above). R represents correlation coefficient.